Journal of Non-Crystalline Solids 355 (2009) 1613–1621

Contents lists available at ScienceDirect

Journal of Non-Crystalline Solids

journal homepage: www.elsevier.com/locate/jnoncrysol

Morphological and chemical characterization of weathering products on buried Sasanian glass from central Iraq

Monica Gulmini [a,*], Marco Pace [a,1], Gabriella Ivaldi [b], Mariamaddalena Negro Ponzi [c], Piero Mirti [a]

[a] Università di Torino, Dipartimento di Chimica Analitica, via Giuria 5, 10125 Torino, Italy
[b] Università di Torino, Dipartimento di Scienze Mineralogiche e Petrologiche, via Valperga Caluso 35, 10125 Torino, Italy
[c] Università di Torino, Dipartimento di Scienze Antropologiche, Archeologiche e Storico-territoriali, via Giolitti 21/e, 10123 Torino, Italy

ARTICLE INFO

Article history:
Received 21 July 2008
Received in revised form 28 May 2009
Available online 3 July 2009

PACS:
68.37.Hk
61.43.Fs
81.70.Pg
82.80.−d

Keywords:
Chemical durability
Archaeology
SEM S100
Scanning electron microscopy
Soda-lime–silica

ABSTRACT

This paper discusses the morphological and chemical features of the weathering products on Sasanian glass finds excavated at the ancient Sasanian town of Veh Ardašīr, some 30 km south of Baghdad (Iraq), and dated from the third to the sixth century. All the considered fragments represent soda-lime glass, with MgO contents between 3% and 8%, resulting from the use of soda-rich plant ash as a flux; within this general frame, two productions can be distinguished due to their MgO to K_2O ratio. Four main alteration typologies were observed by visual examination of the excavated samples; these were studied by scanning electron microscopy, energy dispersive X-ray analysis, inductively coupled plasma-mass spectrometry, X-ray diffraction and thermal analysis. Different alteration features were generally observed for samples belonging to the two compositional groups. In particular, samples with higher MgO to K_2O ratios show definitely thinner crusts, associated with alteration plugs going down into the glass. Moreover, gray or black crusts are related to the presence of manganese at significant levels in the original glass.

1. Introduction

Numerous factors act simultaneously in promoting decomposition of silicate glass: these include glass characteristics (mainly composition, but also thermal history and surface features), as well as environmental factors, with water playing a primary role.

A generally accepted simplified picture of glass weathering accounts for the presence of two degradation pathways: leaching of the modifying cations and network dissolution [1–6]. Leaching can be described as a reaction between inward-diffusing water with non-bridging oxygen atoms; hydroxyl ions are produced by this reaction, which migrate out of the glass together with alkali cations. In the presence of an acid solution, the alkali ions escape the glass network due to an ion exchange reaction with hydrogen ions. A depletion of alkali ions occurs in both cases, although the silica network remains intact, and a gel layer of hydrated silica is formed.

In an alkaline environment, which can develop as a consequence of the leaching process, hydroxyl ions attack bridging oxygen atoms disrupting the silica network; this reaction produces new hydroxyl ions that further accelerate the network disruption until silicon is released into solution. For soda-lime–silica glass this process becomes relevant above pH 9, while for lower pH values the leaching of alkali ions prevails.

Chemical changes begin on the surface of the glass and can then proceed inwards. Besides the pH of the leaching solution, glass composition plays the major role in determining the kind of the surface which forms on the glass in contact to natural environments. In the so called durable glass, the gel layer depleted in alkalis, which maintains its silica network undamaged, prevents the advance of the weathering front. In other cases, the gel layer which forms cannot act as a protective film, therefore allowing the weathering processes to proceed inwards into the bulk [4].

Although the main decay mechanisms have been empirically elucidated, modeling the behavior of a glass exposed to a natural environment remains a challenge [7,8]; therefore historical and archaeological glass offers a unique opportunity for checking theoretical treatments of glass deterioration and may help, as an example, to predict the long term behavior of vitrified waste matrices [9].

* Corresponding author. Tel.: +39 011 6707618.
E-mail address: monica.gulmini@unito.it (M. Gulmini).
[1] Present address: Agenzia Regionale per la Protezione Ambientale (ARPA) Piemonte, Via Pio VII 9, 10135 Torino, Italy.

0022-3093/$ - see front matter © 2009 Elsevier B.V. All rights reserved.
doi:10.1016/j.jnoncrysol.2009.05.056

Chemical changes during burial adversely affect investigation on provenance, technology of production and use of an artefact; the knowledge of the characteristics of the corrosion products does not overcome these drawbacks, nevertheless it may help to choose the most suitable conservation treatment.

Moreover, from an archaeological point of view, post-depositional modification confuses the interpretation of the finds, whose original appearance is obscured by opaque crusts of decay products; archaeologists may therefore wonder whether a relation exists between the original composition of the glass and its aspect on excavation. Of course, because of the strict dependence of corrosion products on burial environment, a general answer cannot be found; nevertheless, the final appearance may be possibly related to composition for glass finds excavated at the same site, since in this case similar environmental conditions can be assumed.

The present work reports the results obtained by studying the degradation products on 15 samples of archaeological glass by use of various techniques; 39 specimen were further used to verify the conclusion drawn from this study on the 15-sample set. All the samples were selected from the *corpus* of fragmentary vessels and raw glass excavated at the archaeological site of Veh Ardašīr, some thirty kilometers south of Baghdad in modern Iraq.

Veh Ardašīr was founded in the first half of the third century on the west bank of the river Tigris by the first Sasanian king Ardašīr. The glass fragments considered here were excavated from similar archaeological contexts in the so called "artisans' quarter", near the south-western wall, where the presence of numerous coins allowed archaeologists to reliably date the strata. They were selected in order to cover the entire time span of the Sasanian presence in this part of the town (from the third to the sixth century), and all the varieties of weathering crusts observed [10,11].

Sasanian glass differentiates from the contemporary silica–soda-lime western production because of higher potassium and magnesium oxides contents (above 3 wt%), deriving from the use of plant ash as a source of alkalis [12–15]. Glass obtained using soda-rich ash is often referred to as high magnesium glass (HMG), in contrast to low magnesium glass (LMG) produced by use of soda-rich evaporite minerals, which leads to potassium and magnesium oxides contents mainly below 1 wt% [16].

The weathering of buried LMG glass is fairly well documented [17–22], whereas less work was devoted to the study of plant-ash soda glass [5,23]. The aim of this paper is to contribute to fill the lack of information on degradation products for HMG productions excavated from the humid Mesopotamian environment; in fact, HMG finds excavated from dry environments (e.g., the Egyptian desert) are well preserved and do not show the thick degradation crusts found on the Iraqi archaeological samples [5].

All of the fifteen samples considered here were first observed under a stereomicroscope and then investigated by scanning electron microscopy coupled with an energy dispersive X-ray detector (SEM-EDS). Degradation crusts from some of them were further subjected to X-ray diffraction (XRD), inductively coupled plasma-mass spectrometry (ICP-MS) and thermogravimetry (TG).

2. Experimental

Within the frame of a larger work on glass production in central Iraq during the first millennium AD [12,13], it was possible to observe macroscopically the variety of decay crusts on a set of about 60 glass finds (fragmentary vessels, chunks of raw glass and waste glass) excavated at Veh Ardašīr and dated from the third to the seventh century AD. This led to the identification of four main groups as concerns the visual appearance of the degradation products.

A first group (visual group 1) consists of samples coated by a thick, light brown, matt crust, sometimes dark stained, that easily flakes away leaving an iridescent and pitted surface beneath; a second one (visual group 2) collects samples featuring a generally thick, whitish compact crust, sometimes dark stained, which is more adherent to the glass with respect to the crust of group 1. A further group (visual group 3) is characterized by a thin whitish patina with mother-of-pearl lustre, firmly adherent to the glass; the last group (visual group 4) is made up of samples featuring either a thin, adhering gray crust or a thick, flaking black one.

Fifteen samples were selected among fragmentary bowls, bottles, vases, beakers and chunks of raw glass in order to represent all the above groups, in view of a deeper investigation on the morphology and the composition of the alteration products. Table 1 summarizes the most relevant features of each of the considered fragments and Fig. 1 shows samples representative of each visual group.

Samples for analysis were cut from each archaeological find by use of a diamond-coated rotary micro-tool. In most cases, it was possible to obtain the degradation crust attached to the pristine

Table 1
Details of the analysed samples. See text for a description of the visual groups of decay products and typology of the unaltered glass.

Sample	Inventory number	Visual group of decay products	Pristine glass type	Ref.
VA05	V 2585	1	Sasanian 1	[12]
VA08	V 3029	3	Sasanian 2	[12]
VA09	V 3030	3	Sasanian 2	[12]
VA10	V 3607	1	Sasanian 1	[12]
VA17c	(a)	2	Sasanian 1	[12]
VA22	V 1596	3	Sasanian 2	[10,12]
VA30	V 4534	4	Sasanian 2	[12]
VA35c	(a)	1	Sasanian 1	[12]
VA46	V 8132	2	Sasanian 1	[13]
VA63	V 506	4	Sasanian 1	[13]
VA70	V 8194	4	(b)	[13]
VA74	V 8191	2	(b)	[13]
VA80	V 326	4	Sasanian 1	[13]
VA83	V 325	3	Sasanian 1	[13]
VA89	V 8163	3	Sasanian 2	[13]

(a) Chunk of raw glass; (b) attributed to neither group.

Fig. 1. Examples of alteration products on samples assigned to visual group 1 (above, left), 2 (above, middle), 3 (above, right), 4 (below). The two samples of visual group 4 illustrate the varieties of homogeneously black or gray alteration products.

glass; these samples were mounted in epoxy resin, abraded with silicon carbide papers and then polished with diamond pastes. The polished sections were examined under reflected light at 4–60× magnification by a stereomicroscope equipped with a digital video camera, in order to observe the unaltered glass color and the coarse structure of the weathering crust; they were finally coated with a thin carbon layer to make them suitable for SEM-EDS investigation.

Cross sections of the glass attached to alteration products could not be obtained for two out of the three investigated fragments of group 1, since the weathering crust flaked away from the glass surface on cutting. In these cases, the glass was embedded into epoxy resin while the crust flakes were fixed on a microscope plate and morphologically observed both by optical and electron microscopy, in the latter case after carbon coating.

Pure, certified compounds were used for the EDS analysis of the alteration crusts and for determining potassium, phosphorus, sulfur, chlorine, iron, manganese and titanium levels in the unaltered glass. Silicon, sodium, magnesium, calcium and aluminum were quantified in the pristine glass by using NIST SRM 620 (soda-lime glass) as the quantification standard. The composition of the unaltered glass was determined as the mean of the results achieved by scanning the electron beam on three different sample areas (40x60 μm^2) within each sample; data from each analytical run, expressed as weight percentage of element oxide, were recast to 100%. The accuracy was evaluated by analyzing standard reference glasses (SGT07 and SGT10) and was generally better than 3% for sodium, magnesium, aluminum, silicon, and calcium oxides; the contents of the other elements were below or near to the instrumental detection limits in these reference glasses. The composition of the alteration crusts was either investigated by beam scanning or by spot analysis; in the latter case the electron beam was focused on areas of about 5 μm diameter. X-ray maps were further recorded on selected areas to elucidate elemental distributions within the crusts.

Portions of some of the weathering crusts were powdered in an agate mortar to be used for X-ray diffraction, thermogravimetry and inductively coupled plasma-mass spectrometry analysis.

XRD patterns were recorded using the powder technique on the degradation crust of samples VA05, VA08, VA10, VA46, VA63 and VA80 (graphite monochromatized Cu Kα radiation at 1.54278 Å was employed as a primary beam). Diffraction patterns were recorded at room temperature in the 4–70° 2θ range, at a 0.02 scan rate, with a 14 h total accumulation time (16 s per step).

ICP-MS analyses were performed on the degradation crusts of samples VA05, VA35c, VA46, VA63, VA74 and VA80. Group 3 could not be represented here, because the thin, adherent crust did not allow one to obtain a quantity of decay products suitable for the analysis. The finely pulverized samples were dissolved by alkaline fusion before ICP-MS analysis. Details on the procedure and instrumental settings are reported elsewhere [13].

Portions of the powdered crusts analyzed by ICP-MS were further subjected to TG within the temperature range 30–900 °C (15 °C min^{-1}).

3. Results

3.1. Unaltered glass composition

The composition of the pristine glass determined by ICP-MS analysis is reported in [12] and [13]. Results of the SEM-EDS analyses performed in this work are reported in Table 2. As previously found [12,13] the investigated samples are soda-lime–silica glasses, whose MgO and K_2O levels suggest the use of soda-rich plant ash as the alkali source. Moreover, two different compositions were recognized, mainly due to a different magnesium content. One of these (Sasanian 1) is found across the whole Sasanian epoch and features MgO contents roughly between 3 and 5 wt% and MgO/K_2O ratios below 1.5; the other one (Sasanian

Table 2
Composition of the unaltered glass determined by SEM-EDS (wt%). Glass typology (Sasanian 1, 2 or neither of them) is indicated in brackets under sample name. Relative standard deviations are also reported. n.d. indicates that the mean of the results was below the detection limit, i.e.: 0.2 wt% P_2O_5, 0.2 wt% MnO, 0.1 wt% TiO_2.

	SiO_2	Na_2O	K_2O	CaO	MgO	Al_2O_3	Fe_2O_3	MnO	TiO_2	P_2O_5	Cl	SO_3
VA05	63.1	18.7	4.31	5,75	3.55	2.06	1,05	n.d.	n.d.	n.d.	0.87	0.49
(1)	(0.2)	(0.1)	(0.09)	(0.05)	(0.08)	(0.05)	(0.08)				(0.04)	(0.05)
VA08	59.8	18.7	3.85	5.53	7.97	2.1	0.74	n.d.	n.d.	n.d.	0.91	0.3
(2)	(0.2)	(0.1)	(0.03)	(0.09)	(0.05)	(0.1)	(0.04)				(0.05)	(0.1)
VA09	61.5	18.4	4.03	4.9	8.02	1.30	0.46	n.d.	n.d.	n.d.	1.06	0.3
(2)	(0.1)	(0.1)	(0.07)	(0.1)	(0.04)	(0.07)	(0.03)				(0.05)	(0.1)
VA10	62.5	16.3	4.09	6.44	5.21	2.7	0.83	n.d.	0.23	0.28	0.84	0.6
(1)	(0.2)	(0.1)	(0.06)	(0.08)	(0.01)	(0.1)	(0.05)		(0.05)	(0.08)	(0.02)	(0.1)
VA17c	59.0	18.3	5.14	7.39	4.68	2.6	1.35	n.d.	n.d.	n.d.	0.79	0.7
(1)	(0.3)	(0.1)	(0.07)	(0.08)	(0.04)	(0.1)	(0.06)				(0.01)	(0.1)
VA22	59.1	19.6	3.55	5.72	8.21	1.79	0.61	n.d.	n.d.	n.d.	1.12	0.26
(2)	(0.1)	(0.1)	(0.04)	(0.06)	(0.06)	(0.04)	(0.07)				(0.09)	(0.08)
VA30	59.7	17.3	3.4	8.11	8.18	0.95	0.40	0.65	0.22	n.d.	0.66	0.4
(2)	(0.2)	(0.1)	(0.1)	(0.03)	(0.05)	(0.06)	(0.09)	(0.06)	(0.07)		(0.06)	(0.1)
VA35c	64.2	18.1	4.1	4.8	4.64	1.99	0.84	n.d.	n.d.	n.d.	0.78	0.47
(1)	(0.1)	(0.2)	(0.1)	(0.1)	(0.05)	(0.01)	(0.07)				(0.04)	(0.08)
VA46	61.4	17.0	4.39	6.74	3.50	3.21	1.72	n.d.	0.32	0.38	0.82	0.55
(1)	(0.1)	(0.1)	(0.04)	(0.05)	(0.01)	(0.05)	(0.02)		(0.06)	(0.05)	(0.03)	(0.03)
VA63	60.3	17.0	4.83	6.31	3.90	2.16	1.20	2.37	0.24	0.36	0.67	0.66
(1)	(0.1)	(0.1)	(0.04)	(0.01)	(0.02)	(0.04)	(0.01)	(0.04)	(0.02)	(0.04)	(0.02)	(0.03)
VA70	63.5	17.3	3.36	7.09	5.61	0.87	0.36	0.41	n.d.	0.28	0.84	0.47
(neither)	(0.3)	(0.1)	(0.07)	(0.08)	(0.07)	(0.03)	(0.09)	(0.04)		(0.06)	(0.03)	(0.07)
VA74	61.8	18.0	3.54	6.7	5.49	2.20	0.79	n.d.	n.d.	n.d.	1.05	0.5
(neither)	(0.1)	(0.1)	(0.03)	(0.1)	(0.01)	(0.08)	(0.06)				(0.05)	(0.1)
VA80	62.6	17.6	3.5	6.12	4.08	2.3	1.07	1.15	0.14	n.d.	0.98	0.43
(1)	(0.2)	(0.1)	(0.1)	(0.09)	(0.03)	(0.1)	(0.02)	(0.01)	(0.09)	n.d.	(0.07)	(0.06)
VA83	63.8	15.3	4.2	7.4	4.46	2.13	1.01	n.d.	n.d.	0.35	0.96	0.40
(1)	(0.2)	(0.1)	(0.10)	(0.1)	(0.04)	(0.07)	(0.09)			(0.01)	(0.04)	(0.04)
VA89	60.6	18.4	3.28	5.9	7.34	2.11	0.75	n.d.	n.d.	n.d.	1.10	0.5
(2)	(0.4)	(0.1)	(0.02)	(0.1)	(0.01)	(0.03)	(0.03)			n.d.	(0.02)	(0.1)

2), attested from the fourth century onwards, is characterized by MgO contents above 6 wt% and MgO/K_2O ratios higher than 2.

As it results from Table 1, eight out of the samples considered here can be assigned to the Sasanian 1 compositional group and other five to the Sasanian 2 group. Two more samples, however, cannot be reliably assigned to either group of composition on the basis of their magnesium and potassium contents.

3.2. Compositional and micro-textural features of alteration products

XRD patterns indicate that the degree of crystallinity in the crusts is generally very low. Only for sample VA05 (visual group 1), diffraction peaks emerge from the background, that may confidently be attributed to the presence of halite (sodium chloride) and calcite (calcium carbonate).

SEM observation on polished sections reveals that generally the alteration crusts show finely-laminated structures characterized by various morphologies; EDS analysis of all of these crusts yields data which sum up well below 100% element oxides. Two main factors may contribute to the gap observed (henceforth Δ100). First, EDS analyses do not allow one to know the amount of hydrogen present and therefore water is excluded from the quantified components; second, the sum of the determined oxides is lowered by the presence of voids within the crust. In fact, Δ100 is negligible for the anhydrous, homogeneous pristine glass, but amounts to some 20–50% within the hydrated, porous alteration crusts.

The mean hydration levels in the alteration crusts were estimated by TG, which also revealed their high hygroscopicity; in fact, some milligrams of each crust studied by this technique recovered their original weight in few seconds after having been dried up to 250 °C. The water content was estimated from the loss of weight observed up to 800 °C, where a plateau is reached in the TG diagram; the first derivative of the TG curve always shows a peak within the 30–250 °C range of temperature, that can be attributed to the loss of pore water.

Among the samples studied by this technique, VA05 and VA35C show the greatest weight loss, that amounts to about 12% at 250 °C and about 15% at 800 °C, while samples VA46, VA74, VA63 and VA80 loose about 8–9% of their mass by 250 °C and a total of some 12% at the end of the heating. It may be noted that these figures are significantly lower than those reported for alteration crusts of buried medieval European wood-ash glass [9] and submerged Roman glass [22].

It emerges from the above data, that the Δ100 observed cannot result from the sole presence of water, even more so because embedded samples should loose at least part of their pore water in the vacuum of the SEM sample chamber and due to heating following the impact with the accelerated electrons. One can therefore reasonably assume that voids play the major role in determining the high Δ100 observed within the degradation products; for this reason, compositional data will be henceforth reported after recasting to 100%, in order to allow a direct comparison among them.

Contents of major, minor and trace elements in the decay products were also determined by ICP-MS analysis and compared with those previously obtained for the unaltered glass by the same technique [12,13]. In this context, an open question concerns the way to perform this comparison [4,24], because of the partial substitution of modifiers cations by hydrogen ions in the altered glass. Here, the ratio between the content of each element (molar percentage) in the decay crust and in the pristine glass ($q_{d/g}$) was calculated taking into account the water content in the crust. Values for $q_{d/g}$ are reported in Table 3; they may give evidence on elements leached from the glass or accumulated within the decay products.

Values below unity indicate that the element has been leached out of the glass, leaving a depleted alteration layer. Values above unity, apart from suggesting a possible external contribution, may arise from the removal of other elements, which results in a higher relative content for the considered one.

The general trend for major elements points to a depletion of alkalis and alkaline-earth elements in the alteration crust, while an enrichment is generally evidenced for aluminum, iron, titanium and manganese. As for trace and rare earth elements (data not reported) $q_{d/g}$ are generally above unity, with few exceptions; among these, rubidium and strontium follow the behavior of the other alkaline and alkaline-earth elements.

Other features, which are peculiar to samples assigned to each visual group, are reported in the following sections.

3.2.1. Visual group 1

The examination of crust flakes under the optical microscope shows that the outermost surface looks matt and relatively even, although somewhere pitted and furrowed by black stained cracks, while inner layers show an iridescent gloss and a wavy texture.

SEM images of crust flakes show a micro-porous and fractured structure in the outermost surface as reported in Fig. 2. Crystallites of sodium chloride (a few micrometers across), also detected by XRD, are also observed throughout the crust, and calcium sulfate and phosphate sub-micron particles on the crust surface only.

SEM images of polished cross sections (Fig. 3) show a laminated structure extending throughout the crust thickness. This is thick (up to more than 1 mm) and fissured by cracks that follow preferentially the direction parallel to the unaltered glass surface; this accounts for the tendency of the crust to flake away. Moreover, the outermost portion (approximately 100 μm thick) shows regular layers, almost parallel to each other and to the external surface, while more complex structures characterize the inner part. X-ray maps and SEM-EDS analyses indicate that silica and alumina (some 2 wt% for the latter) are the only components that can be confidently determined, while alkaline and alkaline-earth elements are barely quantifiable (sodium and magnesium) or below the instrumental detection limit (potassium and calcium). Moreover, the external, more regular portion of the crust is characterized by Δ100 values around 50, whereas this drops to about 30 for the inner portions; this suggests a more porous nature of the outermost part when compared with the strata closer to the glass. Finally, X-ray maps highlight the presence of iron and manganese-rich com-

Table 3
$q_{d/g}$ values calculated between elemental levels, expressed as molar percent, in the alteration crust (this work) and in the pristine glass (from Refs [12,13]). For the weathering crust, the content of water was also taken into account when calculating molar percentages. All the fragments but one belong to the Sasanian 1 typology; sample VA74 was not attributed to any typology.

	Visual group of decay products	Si	Na	K	Ca	Mg	Al	Fe	Mn	Ti
VA05	1	0.64	0.08	0.65	0.25	0.25	2.70	2.28	0.85	2.30
VA35c	1	0.68	0.08	0.75	0.11	0.16	2.62	3.43	1.18	3.34
VA46	2	0.90	0.06	0.70	0.23	0.30	1.68	1.58	1.53	1.69
VA74	2	0.95	0.02	0.39	0.32	0.21	2.17	1.87	1.60	1.87
VA63	4	0.82	0.08	0.48	0.23	0.27	1.90	1.70	1.70	1.90
VA80	4	0.86	0.08	0.50	0.11	0.13	0.30	0.62	1.91	1.37

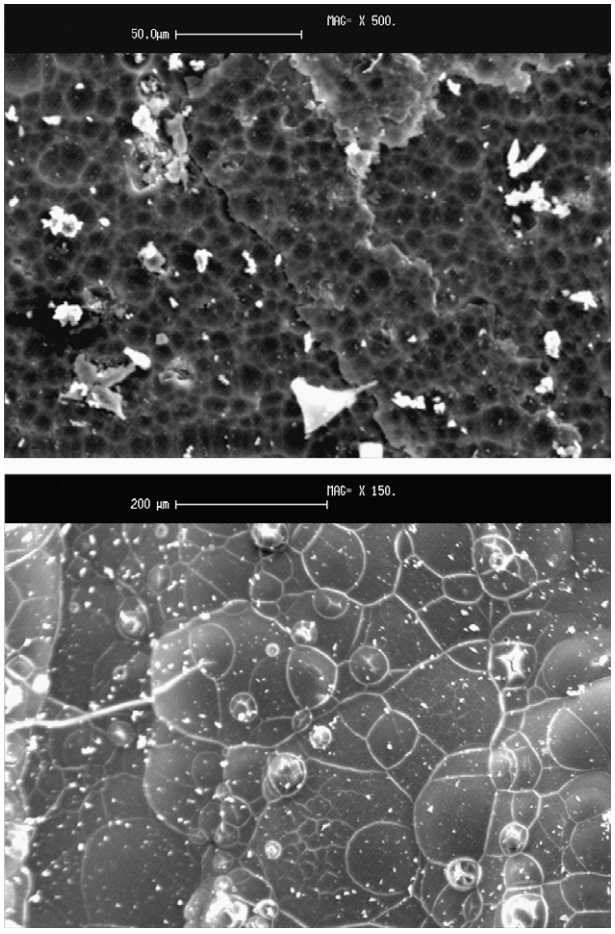

Fig. 2. Secondary electron images of the outermost (above) and innermost surface (below) of a crust flake from sample VA35c.

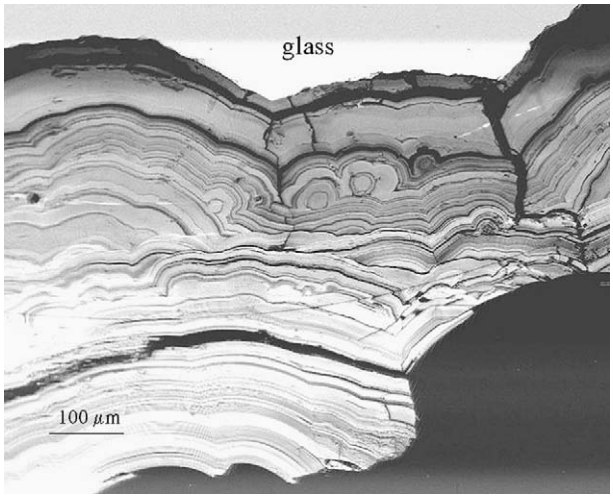

Fig. 3. Back-scattered electron image of a polished section of the crust of sample VA10.

pounds within the outermost part of the crust, that accounts for the dark staining observed by optical microscopy.

3.2.2. Visual group 2

In comparison with the samples of visual group 1, the alteration crust of group 2 appears more compact and homogeneous when observed under the optical microscope. The outermost surface appears smooth and black stained, and that in contact with the pristine glass is characterized by a flat, iridescent surface. Peculiar to this group is the presence of dark spots both on the surface and within the whole thickness of the crust.

SEM images of polished sections indicate that the structure of the alteration products is similar for all the samples attributed to this group. In particular, the crusts show a highly variable thickness within the same sample, ranging from about 50 µm to some millimeters, with cracks crossing them in all directions. Moreover, both regular and complex laminated structures are present, with a distance between the lamellae definitely smaller than that observed for visual group 1 (Fig. 4).

EDS analyses and elemental maps point to a general depletion of alkaline and alkaline-earth elements in the crust; within this general frame, zones less depleted in magnesium are observed for sample VA46 (Fig. 5). High levels of calcium and sulfur are detectable in all the samples inside some of the cracks, and may be attributed to the precipitation of calcium sulphate (Fig. 4). Localized enrichments of manganese (up to 16 wt% MnO), iron and titanium (approximately 5 wt% Fe_2O_3 and 5 wt% TiO_2) are further shown both on the crust surface and within it (Fig 4); they are responsible of the dark staining observed under the optical microscope. The morphology of these compounds, as observed on polished sections, encompasses both relatively extended areas as well as threadlike infiltrations between the lamellae.

3.2.3. Visual group 3

The main characteristic of the samples of group 3 is the presence of a thin patina covering the entire surface of the glass, accompanied by more or less numerous corrosion plugs intruding into it (Fig. 6). One fragment, namely VA83, was included in this group because of its appearance at the naked eye; however, when observed in section under the optical microscope, it shows a thicker crust and the intrusions of decay products that characterize the other samples are not present.

Apart from VA83, SEM images of polished sections show that the thin patina (about 20–200 µm thick) consists of a series of fairly regular lamellae, with plugs of decay products intruding up to several hundreds micrometers into the glass. In most samples, the plugs are characterized by the presence of an external lamellar portion and a "spongy" core (Fig. 6); in one case (VA89), however, the plugs are smaller and less numerous and show a lamellar structure in both borders and cores, although the thickness of the lamel-

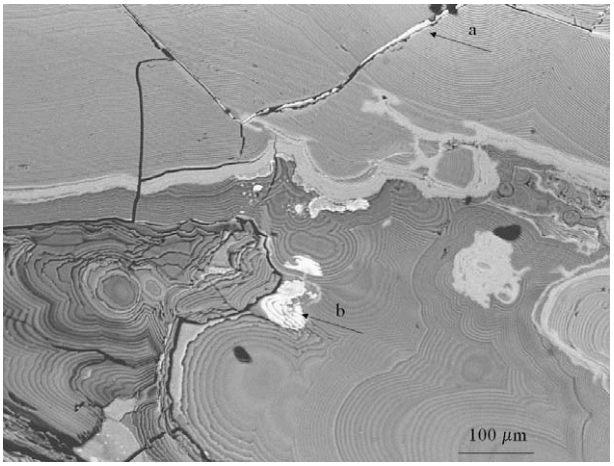

Fig. 4. Back-scattered electron image of the crust of sample VA74, showing cracks filled with calcium sulfate (a) and areas rich in manganese, iron and titanium (b).

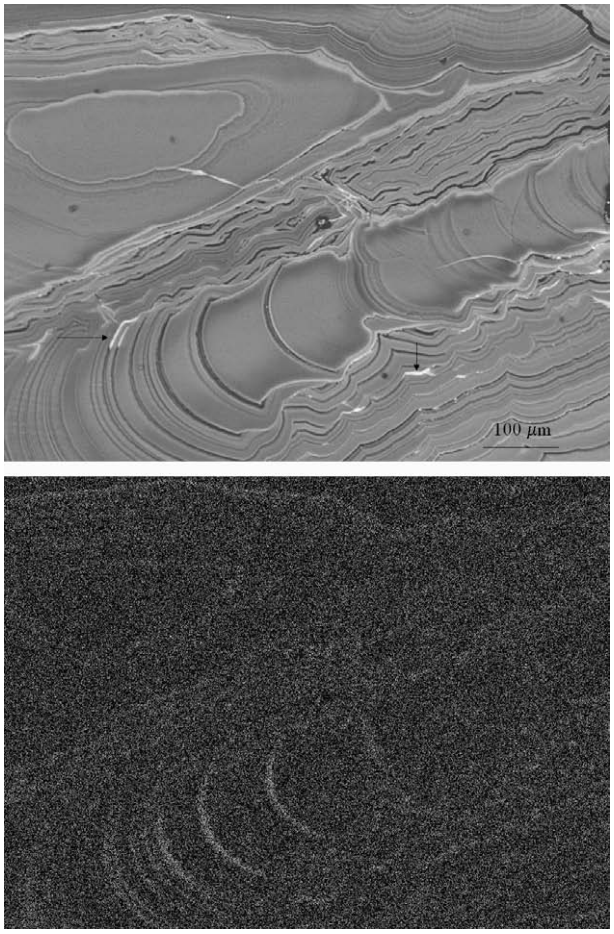

Fig. 5. Back-scattered electron image (above) and magnesium X-ray map (below) showing a laminar distribution for this element within the crust of sample VA46. Infiltrations of manganese-rich compounds (indicated by the arrows) are visible in the back-scattered electron image.

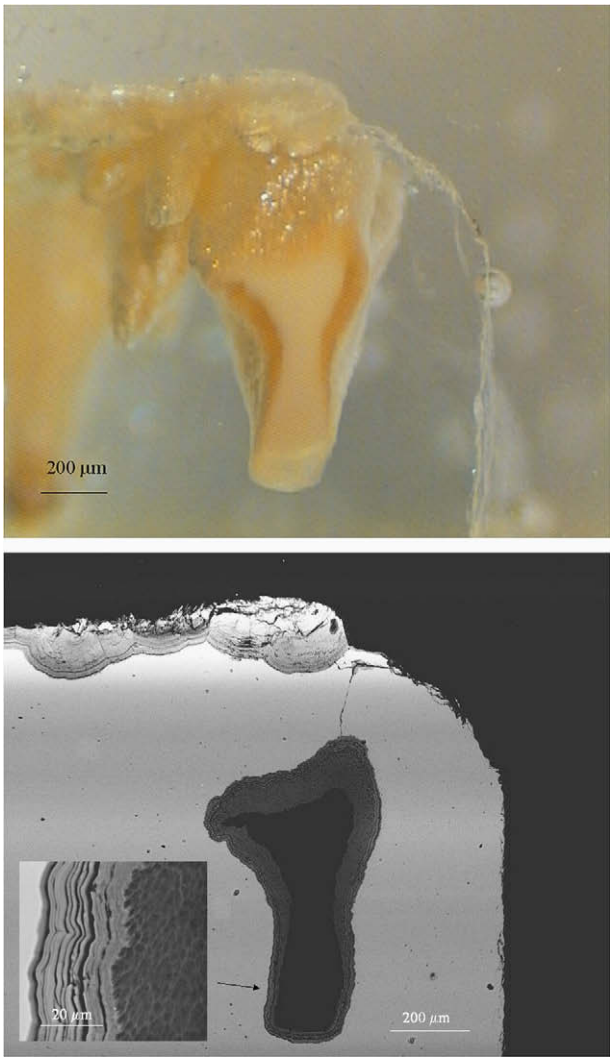

Fig. 6. Optical microscope image of a cross section (above) and back-scattered electron image of a polished section (below) of sample VA08. The latter shows a thin superficial patina and a portion of a plug intruding into the unaltered glass; the insert magnifies a part of the plug in contact with the unaltered glass.

lae is definitely higher in the cores with respect to the borders and the superficial patina.

EDS analysis shows that no significant difference emerges among plug cores, plug borders and superficial patinas for the same sample, once data of composition are recast to 100; in fact, all of them mostly consist of silica, with about 2–5 wt% Al_2O_3, 1 wt% Na_2O and K_2O, and less than 1 wt% CaO and MgO. However, a difference generally emerges between the Δ100 value observed for lamellar areas (about 12) and for "spongy" plug cores (about 25), and this accounts for the different luminosity observed in back scattered electron images. This is not the case for sample VA89, where Δ100 amounts to about 15 for all the observed decay morphologies.

3.2.4. Visual group 4

Under the optical microscope, polished sections of samples of group 4 show decay structures which allow one to take the gray-crusted samples VA30 and VA70 apart from each other and from VA63 and VA80, which show a darker crust. These differences are further highlighted under the electron microscope; in fact, SEM images of samples VA63 and VA80 show a thin (20–50 μm) compact layer superimposed to a lamellar structure advancing into the glass for some 200 μm up to 1 mm; the latter is mainly characterized by a hemispherical front, although more complex structures are also present (Fig. 7). This structure may resemble that observed for groups 1 and 2, but it is characterized by a much larger quantity of black areas, which appear bright in back-scattered electron images; elemental maps further highlight the presence of more or less regular infiltrations within the lamellar structure, characterized by high levels of manganese (Fig. 8).

EDS analysis reveals large compositional variability among different areas of the same crust, mainly due to differences in the manganese content, which may range from below detection limit up to 25 wt% MnO. The other main components of the degradation products are silicon, aluminum and iron compounds, apart from a thin compact, homogeneous superficial patina (Δ100 less than 1), which proves to be only made of silica.

The crust on sample VA30 may be relatively thin (about 50 μm), with a fairly regular hemispherical alteration front, or it may spread up to about 200 μm into the unaltered glass (Fig. 9); these thicker portions show very complex structures, in which relics of unaltered glass are also present. As a whole, the crust shows an irregular front of penetration into the glass, with the presence of preferential points for the decay reactions. This characteristic was also observed for samples of visual group 3, although the morphology of the plugs is better defined there. Elemental maps indicate a general depletion in alkaline and alkaline-earth elements, and highlight a spotty accumulation of manganese, iron and (to a

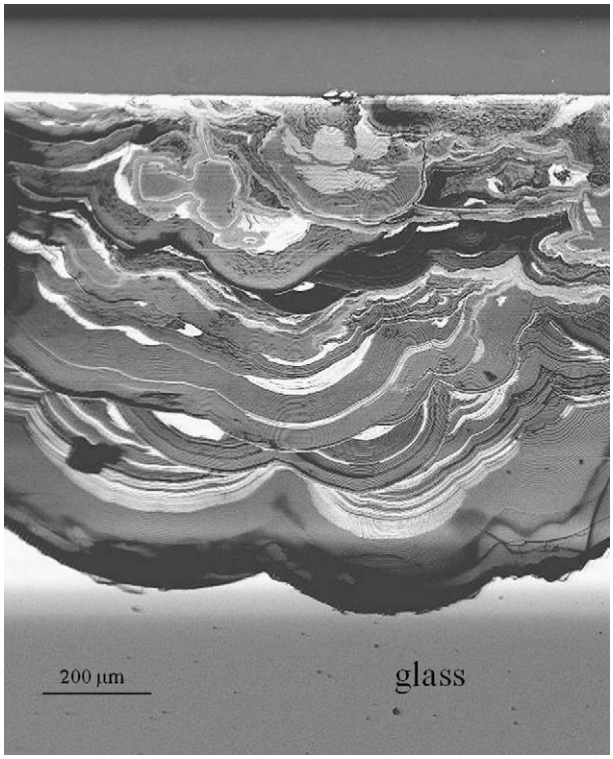

Fig. 7. Back-scattered electron image of a polished section of sample VA63. Light areas appear black when observed under the optical microscope.

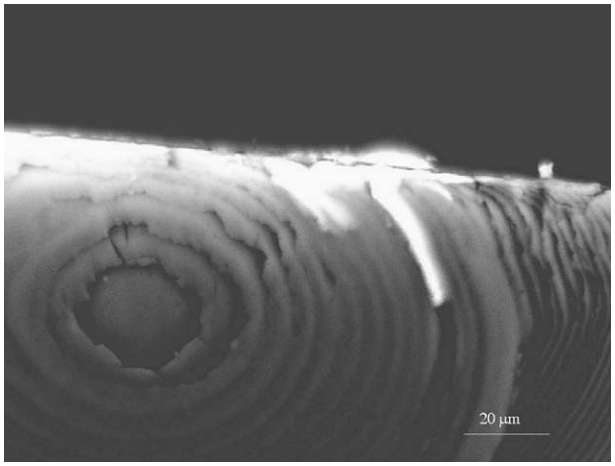

Fig. 8. Back-scattered electron image of a polished section of sample VA80 showing intrusions of manganese-rich compounds (lighter areas) in the lamellar alteration structure.

lesser extent) magnesium compounds, the former two accounting for the gray color of the crust.

As for sample VA70, already mentioned for its peculiar composition, the crust thickness varies from about 150 up to 800 μm and is characterized by complex lamellar systems with ovoidal plugs of more regular structure intruding into it (Fig. 10). Compositional maps do not highlight significant differences between the ovoidal structures and the rest of the decay crust, being both mainly constituted by silica. Nevertheless, areas other than the ovoidal plugs show spotty accumulation of manganese and iron compounds that accounts again for the dark color of the sample surface.

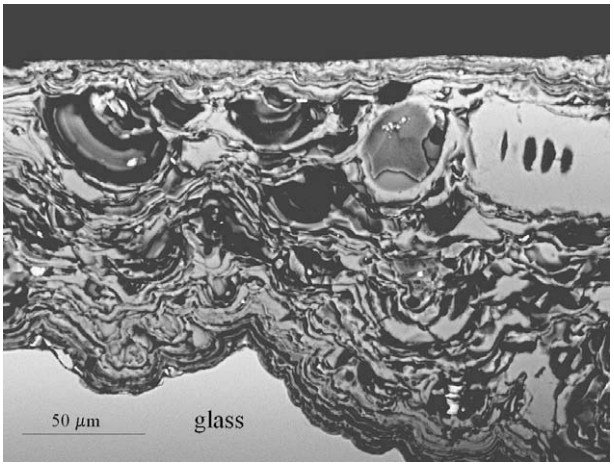

Fig. 9. Back-scattered electron image of a polished section of sample VA30.

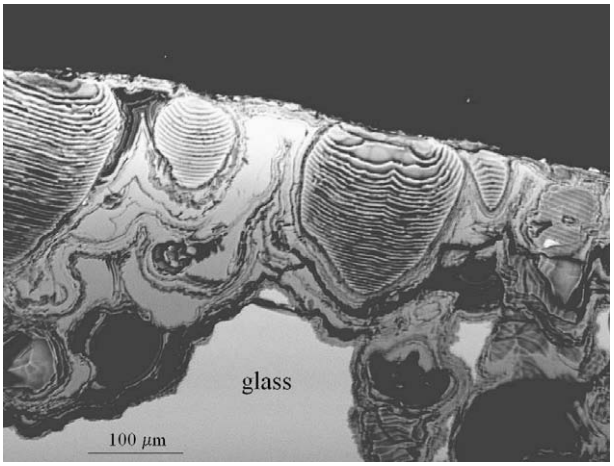

Fig. 10. Back-scattered electron image of a polished section of sample VA70.

4. Discussion

4.1. Visual characteristics of the crust with respect to pristine glass composition

The results obtained point to a possible relation between the glass composition and the visual aspect of the degradation products. In fact, samples of groups 1 and 2, featuring thicker degradation crusts, are characterized by a Sasanian 1 composition (VA74 which shows an intermediate composition, also falls within group 2); in contrast, visual group 3 is formed, with one exception, by samples featuring a Sasanian 2 composition. The only sample of Sasanian 1 composition originally included in group 3 (VA83) actually shows micro-morphological features that differentiate it from the other samples of the group; in fact, the latter generally show a thinner alteration crust, although preferential points of attack lead to plugs intruding more or less deeply into the unaltered glass. The decay products on sample VA83 share with the other samples of group 3 a fairly regular lamellar structure of the surface, which probably accounts for a similar visual effect; however, the different composition may play a role in determining a preferential attack on some areas of the glass, giving rise to the plugs which characterize the micro-morphology of the Sasanian 2 samples.

The occurrence of homogeneous black or gray shades in the crust is always accompanied by manganese levels in the original

glass which lie above the limit of detection of the EDS technique (some 0.2 wt% MnO). Manganese compounds may form within the decay products due to the contribution of Mn(II) ions introduced by environmental solutions, as well as leached out of the glass [25]; oxidation of Mn(II) may then cause the precipitation of Mn(III) or Mn(IV) dark compounds within cracks, pits and lamellar layers. Since the occurrence of a homogeneous gray or black crust is always related to detectable levels of manganese in the unaltered glass, it seems reasonable to assume that the contribution of manganese of internal origin plays a major role in determining the dark color of the crusts in visual group 4. Moreover, the Sasanian 1 samples VA63 and VA80 show micro-morphological features resembling those of the other Sasanian 1 fragments (assigned to groups 1 and 2), whereas the micro-morphology of the Sasanian 2 sample VA30 shows, at least partially, the characteristics of the other Sasanian 2 samples (assigned to group 3).

These considerations may help one in assigning the composition of the pristine glass as Sasanian 1 or Sasanian 2 and in suggesting relatively high levels of manganese within the glass itself. In order to test the reliability of this visual approach, more samples were further considered, including thirty-nine fragments of finished objects and five chunks of raw glass; their composition had been previously determined [12,13], allowing one to assign them to either Sasanian 1 or Sasanian 2 composition or to neither of them. All the fragments of finished objects were subdivided according to their appearance into the four visual groups, and the correspondence between the expected and the actual composition was checked. As for the chunks of raw glass, only three out of five could be included into one of the four visual groups on the basis of their superficial aspect and were considered for further discussion.

Concerning samples with low manganese levels (below 0.2 wt% MnO), 23 out of 26 Sasanian 1 samples were assigned to visual group 1 or 2 and therefore correctly recognized; the other three showed a thin iridescent patina and were therefore attributed to visual group 3, which would suggest, incorrectly, a Sasanian 2 composition (as already occurred for sample VA83). As for Sasanian 2 samples themselves (five fragments), all of them featured the thin, mother-of-pearl patina that characterizes visual group 3. Samples of peculiar composition (five samples) where distributed between visual groups 2 and 3.

As concerns fragments with manganese levels above 0.2 wt% MnO (six samples), five of them developed the dark homogeneous crust peculiar to visual group 4; the other one, featuring a manganese content of about 0.5 wt% MnO and Sasanian 2 composition, was attributed to visual group 1, because, despite its relatively thin crust, neither shows a mother-of pearl lustre nor a dark homogenous color.

4.2. Glass durability

The high variability of the crust thickness, even within the same sample, does not allow a reliable estimation of alteration rates. Nevertheless, since the Sasanian 1 composition characterizes samples with definitely thicker crusts with respect to the Sasanian 2 composition, the latter seems to imply a higher durability.

A triangular diagram, reporting molar percentages of network formers, fluxes and stabilizers, is often used to relate glass composition to its durability [4]. Durable glasses are found near the center of the diagram, and durability decreases when samples move towards areas characterized by lower relative contents of network formers and higher contents of fluxing agents. In the present case, a comparison with literature data would suggest good resistance to weathering effects for Sasanian 1 samples, while the Sasanian 2 ones would result less durable, in contrast with the experimental evidence. In fact, some of the latter contain some 60–65 mol% of network formers, i.e. the lower limit estimated for durable glasses [3,4].

A similar indication comes from the evaluation of the NBO/T parameter (non-bridging oxygen per tetrahedron) [26,27], which is used to represent the degree of polymerization of a silicate melt; a larger number of non-bridging oxygen atoms (higher NBO/T) would point to a lower durability of the glass. For the samples considered here, NBO/T values range from 1.2 to 2.2 for Sasanian 2 samples and from 0.9 to 1.1 for the Sasanian 1 ones; this would point again to a supposed higher durability of the latter composition.

It is a fact, however, that both triangular diagrams and NBO/T values do not take into consideration the flux used (potash or soda), nor the stabilizer present in the glass (magnesia or lime); it seems evident from the results obtained here that different relative amounts of these components may play a role in determining the actual rate of glass alteration.

4.3. Composition of the crust with respect to pristine glass composition

As already stated, the crusts of fragments assigned to visual group 3 (encompassing all the studied samples with Sasanian 2 composition) could not be sampled for the ICP-MS analysis and therefore the following discussion is restricted to Sasanian 1 samples.

Data in Table 3 indicate values of $q_{d/g}$ always well below unity for magnesium and calcium. The presence of lamellae enriched in magnesium in some samples suggests that this element may be incorporated in secondary phases; the same holds for calcium, whose compounds were detected by SEM-EDS within the cracks that furrow the decay crusts. The formation of secondary phases containing high levels of calcium or magnesium may have involved ions leached from the glass itself as well as ions dissolved in natural groundwater. The possible combined contribution of external and internal sources may justify the large variability of the content of these elements within the weathering products of different samples. Data in Table 3 further point to a less tendency of potassium to be leached out of the glass with respect to sodium ions.

A depletion of sodium and calcium within the crust with respect to the pristine glass and a more or less marked enrichment for aluminum, iron and manganese is generally reported for decay products of potash-lime and soda-lime glass [4,9,19,20,22,24,28]; less agreement arises for potassium and magnesium, since either depletion [4,9] or enrichment [20,28] were reported for both of them, or even a pronounced enrichment in potassium in the crust, without mention of the magnesium behavior [22]. A thorough work on the decay of archaeological soda-lime medieval glass further suggests that sodium may be more easily leached out of the glass, or less easily incorporated in the decay phases, with respect to potassium [24]. These results are in accordance with those found in the present work, but seem in conflict with the documented higher tendency towards degradation for potash glass with respect to soda glass [3,9,19]. The lower durability of potash glass is generally explained by the higher mobility of potassium ions due to their lower charge to radius ratio with respect to sodium ions, that leads to a dissolution rate for potassium-rich buried glass about one order of magnitude higher than that of sodium-rich glasses [9]. However, the greater packing density of oxygen atoms in a soda-rich glass network with respect to a potassium rich one would lower the diffusion coefficient of potassium ions, since they have to migrate through a lattice with a molar volume reduced by the smaller sodium ions [29].

Within a frame of a common composition, the Sasanian 1 fragments develop a variety of decay products, which differs from a micro-morphological point of view as well as on a compositional

base (Table 3). In fact, the decay products of group 1 show the highest level of hydration as well as the highest relative enrichment in iron, titanium and aluminum, which, incorporated from solutions circulating in the burial environment, probably accounts for the light brown color of the crust. Dark compounds rich in manganese were found only on the surface of the crust of the samples of this group, and this accounts for the lower $q_{d/g}$ values observed with respect to the other samples, where manganese compounds are spread within the whole thickness of the crust.

5. Conclusion

Four main typologies of decay products have been observed on Sasanian glass finds excavated at the archaeological site of Veh Ardašīr. Visual examination of the weathering crust represents, in most cases, a way for assigning the finds to one out of the two main groups of composition of glass circulating in the area during the Sasanian rule. The two productions, which mainly differentiate from each other because of a different MgO to K_2O ratio, generally lead to different visual features of the decay products, and this may help archaeologists in assigning finds to a specific production. The presence of manganese at a significant level in the original glass can be further revealed by the crust aspect, which presents a homogeneous black or gray color.

Moreover, the two different compositions seem to determine a different durability, which, however, does not appear to be predictable by usual approaches such as triangular diagrams or degree of polymerisation.

Acknowledgments

Authors wish to thank Dr. Anna Piccirillo for having performed TG measurements and Dr. Roberto Cossio for his kind help in SEM-EDS analysis. Financial contribution of the Italian Ministry of Instruction and Scientific Research (MIUR) is also acknowledged.

References

[1] R.J. Charles, J. Appl. Phys. 29 (1958) 1549.
[2] H. Scholze, J. Non-Cryst. Solids 52 (1982) 91.
[3] A.M. Pollard, C. Henron, Archaeological Chemistry, The Royal Society of Chemistry, 1996, p. 149.
[4] R. Newton, S. Davison, Conservation of Glass, Butterworth Heinemann, 1996, p. 135.
[5] I.C. Freestone, in: D.R. Brothwell, A.M. Pollard (Eds.), Handbook of Archaeological Sciences, John Wiley, 2001, p. 615.
[6] B. Dal Bianco, R. Bertoncello, L. Milanese, S. Barison, J. Non-Cryst. Solids 343 (2004) 91.
[7] M. Aertsens, D. Ghaleb, J. Nucl. Mater. 298 (2001) 37.
[8] R. Conradt, J. Nucl. Mater. 298 (2001) 19.
[9] J. Sterpenich, G. Libourel, Chem. Geol. 174 (2001) 181.
[10] M.M. Negro Ponzi Mancini, in: R. Boucharlat, J.F. Salles (Eds.), Arabie oriental, Mésopotamie et Iran méridional de l'Age du Fer au début de la période islamique, Recherches sur le Civilisations, 1984, p. 33.
[11] R. Venco Ricciardi, M.M. Negro Ponzi Mancini, in: Coche, la terra tra i due fiumi. Vent'anni di archeologia italiana in medio oriente. La Mesopotamia dei tesori (Catalogo della mostra Torino, Firenze, Roma), Il Quadrante, 1985, p. 100.
[12] P. Mirti, M. Pace, M. Negro Ponzi, M. Aceto, Archaeometry 50 (2008) 429.
[13] P. Mirti, M. Pace, M. Malandrino, M. Negro Ponzi, J. Archaeol. Sci. 36 (2009) 1061.
[14] R.H. Brill, Chemical analyses of early glass, in: The Corning Museum of Glass, vol. 1, 1999, p. 82, vol. 2, p. 151.
[15] R.H. Brill, in: D. Whitehouse (Ed.), Sasanian and Post-Sasanian Glass in the Corning Museum of Glass, Appendix 2, The Corning Museum of Glass, 2005, p. 65.
[16] J. Henderson, The Science and Archaeology of Materials, Routledge, 2000.
[17] G. Salviulo, A. Silvestri, G. Molin, R. Bertoncello, J. Archaeol. Sci. 31 (2004) 295.
[18] P.B. Vandiver, in: D.E. Clark, B.K. Zoitos (Eds.), Corrosion of Glass, Ceramics and Ceramic Superconductors, Noyes, 1992, p. 393.
[19] G.A. Cox, B.A. Ford, J. Mater. Sci. 28 (1993) 5637.
[20] K. Janssen, A. Aerts, L. Vincze, F. Adams, C. Yand, R. Utui, K. Malmqvist, K.W. Jones, M. Radtke, S. Garbe, F. Lechtenberg, A. Knöchel, H. Wouters, Nucl. Instr. and Meth. B 109/110 (1996) 690.
[21] F. Branda, G. Laudisio, A. Costantini, C. Piccioli, Glass Technol. 40 (1999) 89.
[22] A. Silvestri, G. Molin, G. Salviulo, J. Non-Cryst. Solids 351 (2005) 1338.
[23] R. Bertoncello, L. Milanese, U. Russo, D. Pedron, P. Guerriero, S. Barison, J. Non-Cryst. Solids 306 (2002) 249.
[24] J. Sterpenich, PhD thesis, UHP Nancy 1, Altération des vitraux médiévaux, Contribution à l'étude du comportement à long terme des verres de confinement, 1998, available from: <http://tel.ccsd.cnrs.fr/documents/archives0/00/00/76/65/index_fr.html>.
[25] D. Watkinson, L. Weber, K. Anheuser, Archaeometry 47 (2005) 69.
[26] B.O. Mysen, Structure and properties of silicate melts, in: W.S. Fyfe (Ed.), Developments in Geochemistry, Elsevier, 1988.
[27] J. Sterpenich, G. Libourel, J. Non-Cryst. Solids 352 (2006) 5446.
[28] K.J.S. Gillies, A. Cox, Glastech. Ber. 61 (1988) 75.
[29] R. Kirchheim, J. Non-Cryst. Solids 272 (2000) 85.